Measurement-based Model for Water Content Estimation in Sustainable Granular Materials using an IoT Custom Device

N. Papini, L. Rugini, *Member, IEEE*, M. Cecconi, A. Scorzoni, A. Tarantino, and P. Placidi, *Senior Member, IEEE*

Abstract—Soil water content has a primary importance in several scientific fields involving the geotechnical, hydrological agronomic, ecological, and biological properties of the soil mass. In recent years, several techniques for determining soil water content in the laboratory and situ have been proposed and developed. Applying these techniques and adopted measurement systems to different soil types is widely discussed in the literature, thus highlighting a nontrivial issue deserving further experimental research. This paper presents the results of applying a capacitive sensor originally developed for soil water content measurement to sustainable granular materials. In particular, the application regards coffee ground samples with two grain size distributions prepared dry and at increasing Gravimetric Water Content (GWC), at different initial voids ratios. This paper presents a measurement-based analytical model for estimating the water content using low-cost low-frequency IoT sensors. The proposed model estimates the water content exploiting both capacitance and conductance measurements of the parallel electrical model. The obtained results show that including conductance measurements improves the water content estimation, with respect to using capacitance measurements only.

Index Terms—Soil Water Content (SWC); Low-Cost and Low-Frequency IoT Sensors; Sustainable Granular Materials; Measured-based models; Gravimetric Water Content (GWC); Material Density and Grain Size Distribution.

I. INTRODUCTION

S PENT ground coffee represents an agro-industrial residue deriving from coffee consumption. It is counted that more than $2 \cdot 10^6$ t of coffee residues (e.g., coffee ground, pulp, and husk) are produced per year worldwide. Ground coffee is mainly composed of cellulose, lignin, and hemicellulose, while iron, aluminum, copper, manganese, potassium, and cobalt are the main mineral composition of spent coffee grounds covers [1]. Residues of coffee can be used as a renewable energy source [2], agricultural applications [3] and for soil improvement [4], due to the mineralogical composition of the material and its chemical reaction with amorphous composites based on calcium and silica in an alkaline environment. More recently, spent ground coffee was used for ground reinforcement of silty soils, in combination with polypropylene fibers [5]. Therefore, the possible reuse of spent ground coffee in geotechnical engineering applications, such as backfill material for embankments, is gradually increasing in favor of a circular economy perspective. For these earthworks, the estimate of water content and its evolution with time through an in-situ monitoring system is relevant. From an electrical point of view, water content measurements are performed by estimating first the soil permittivity, and then by correlating the results with the water content. Additional information, such as soil density, porosity, and permittivity of the soil solid fraction, is also included. Another reason for choosing exclusively ground coffee in the present paper is due to its physical properties, which avoid or at least limit some difficulties in controlling operating conditions, such as the accumulation of water on the bottom of the sample holder or significant air gaps. Thus, sample preparation in a controlled laboratory environment is simplified for ground coffee, making it a suitable granular material for the experimental characterization of a new sensor.

Concerning water content measurements in ground coffee, some reference values of permittivity can be found in [6], for a wider range of applied frequencies (from 75 kHz to 5 MHz). The authors of [6] investigated the influence of bulk density at the same water content and found that both the real and imaginary components of the complex permittivity decrease as the frequency increases for all moisture contents. The real relative permittivity ranges from 2.25 to 4.5, whereas the conductivity spans from 1 µS/cm to 55 µS/cm. Electrical permittivity is also reported in [7] where coffee and several coffee-soybean mixtures are considered at a single frequency equal to 10 kHz. In this case, the real relative permittivity is in the range 1.3 - 4.3 whereas the electrical conductivity spans from 0.11 µS/cm to 0.87 µS/cm depending on the mixture roasting temperature and soybean powder concentration. In our work, we do not estimate directly the sample permittivity, but we propose a model to estimate directly the water content from the measured capacitance and conductance of the parallel electrical model, both related to the soil dielectric constant and electrical conductivity.

Sensors for water content measurement in a medium such as

---

mail: pisana.placidi@unipg.it).

A. Scorzoni (retired) was with the Department of Engineering, University of Perugia, 06125 Perugia, Italy.

A. Tarantino is with the Department of Civil and Environmental Engineering. University of Strathclyde, Glasgow, UK

soil are of primary importance for analyzing and predicting its behaviour, in both saturated and unsaturated conditions. In the last twenty years, significant advancements have been made for laboratory and in situ-testing using sensors, as demonstrated by the significant literature also focused on different applications [8]-[11]. Soil Water Content (SWC) sensors can be divided into two main families: i) remote sensors that are placed on air/spatial platforms such as drones, small aircraft, or satellites; ii) ground-based sensors typically deployed in stand-alone architectures or a network configuration, e.g., in the Internet of Things (IoT) systems. In IoT applications, a wide number of sensitive nodes are deployed on the field sending data to a central station, monitoring environmental parameters with a big impact on the water footprint in the framework of Precision Agriculture [12].

Among ground-based sensors, we mention soil moisture probes like Time Domain Reflectometers (TDR) and impedance sensors, such as capacitive [13]-[15] and resistive sensors. TABLE I compares the sensor proposed in this work with other ground-based devices found in the literature. The metrics we used are sensor type, operating frequency, cost of the sensor/system, and system portability to perform monitoring activities on the field.

TABLE I
COMPARISON OF THE PROPOSED SENSOR WITH OTHER DEVICES.

Reference	Type	Frequency	Cost	Portability
[15]	Capacitive	1 kHz	N.D.	No
[16]	Capacitive	40 MHz	~10 $	Yes
[17]	Capacitive	1.5 MHz	~2.5 $	Yes
[18]	Capacitive	20 kHz	~31 $ (S.C.)	Yes
[19]	Capacitive	30-180 MHz	~3.0 $	Yes
[20]	Impedance	13.56 MHz	N.D.	Yes
[21]	TDR	S.D.	140.0 $	No
Proposed, [13]	Capacitive	10–100 kHz	~1.7 $	Yes

N.D. = Not Declared; S.C. = System Cost; S.D. = Soil Dependent

The use of TDR in an agriculture application is analyzed in [22] and deeply characterized for water content estimation. In [21] the authors compare the TDR performances with a capacitive probe and highlight that applying these techniques to soils with different physical and geotechnical properties is still an open question worth further investigation and experimental activities. In particular, the effects of such measurements of various soil-specific parameters such as mineralogical composition, soil fabric and structure, and salinity, are critically discussed. In [23] the impact of common properties of granular materials, such as particles dimension and compaction, on impedance measurements performed in sustainable soil, is analysed. The measurements are performed by using a new interdigital capacitive sensor that operates in the frequency range between 10 kHz and 100 kHz. The sensor performance is also analysed by considering soil samples reaching the water saturation condition.

In this paper, we extend the results reported in [23] with detailed insights on:
– a new sample preparation procedure that allows us to reduce as much as possible the unpredictable caffeine dissolution;

– the electrical conductivity impact on the sensor capacitance and conductance in unsaturated samples;
– a new measurement-based model for both capacitance and conductance, as a function of the GWC. The proposed model uses basic functions whose parameters are determined by using a Least Squares (LS) fitting approach. Details about the computational cost of the GWC estimation are reported in Section V.B. By means of the proposed model we estimated the GWC in five different contexts (depending on the sample properties) starting from the measured values of capacitance and conductance. The estimated GWC (EGWC) shows a good agreement with the water content measured during the preparation of different samples featuring distinctive properties.

II. INTERDIGITAL CAPACITIVE SENSOR FOR SWC

Our research aims to verify the proper operation of a low-cost, low-frequency, and low-power T-shaped sensor (see Fig. 1-(a)) built using commercial low-cost PCB double-sided technology. The readout electronics is based on a low-frequency (10 kHz - 100 kHz) and low-cost complete digital impedance meter, that could easily be integrated with a transceiver, to realize a stand-alone IoT node. Details about the architecture and the performance of the implemented readout system can be found in [13] and [24]. Different measurements were carried out to check the system accuracy by comparing its results with those obtained with the same expensive and bulky laboratory instrument described in Section III.A. The equivalent impedance of the sensor in the air and waters with different conductivities highlighted a maximum error of +6.12% for the capacitance and +5.6% for the conductance. Comparing the proposed sensor with the capacitive sensors reported in TABLE I, our system is the only one which measures at the same time the real and imaginary parts of the sensor admittance with the aim of extracting the two components of the complex dielectric constant. The present work is the only one exploiting a low-cost capacitive device with organic material, e.g., ground coffee, and with different granulometry.

In this paper, we focus on the sensitive element performance whose layout is based on two couples of electrodes with an interdigital architecture to maximize the performance of the device in terms of sensitivity. The sensitive element (see Fig. 1-(b) and -(c)) takes the form of a laminated sandwich structure of conductive and insulating layers. The patterned electrodes placed on the top are short-circuited with those on the bottom by using vias and they can be electrically contacted using a pair of custom pads (grey regions#1 and#2, respectively, in Fig. 1-(b)) housed on both sides of the structure. Sect II of [23] reports a detailed description of the sensitive elements' geometrical dimensions. The equivalent admittance of the probe is:

$$Y_X = Y_{Re}(\varepsilon^*_{med}, \varepsilon^*_{PCB}) + jY_{Im}(\varepsilon^*_{med}, \varepsilon^*_{PCB}) \qquad (1)$$

where $j = \sqrt{-1}$ is the imaginary unit and $Y_{Re}(\varepsilon^*_{med}, \varepsilon^*_{PCB})$, and $Y_{Im}(\varepsilon^*_{med}, \varepsilon^*_{PCB})$ are the real and imaginary parts of the admittance, respectively. The last two terms are a function
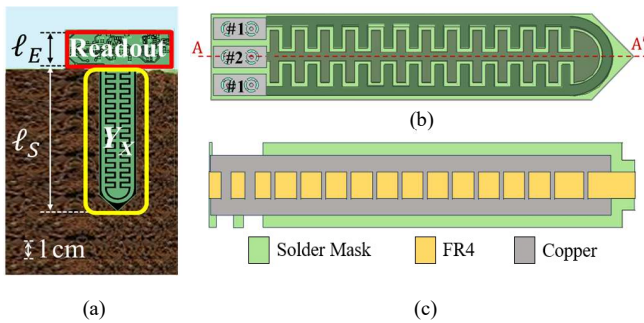
Fig. 1. (a) Node Sensor layout (ℓ_E=2 cm, ℓ_S=9 cm); (b) Sensitive element layout: electrodes #1 and #2 are represented by the three regions in gray; (c) AA' cross-sectional view (b)).

Fig. 2. Experimental setup: (a) LCR-meter (model HP4275A), and (b) geometry of the laboratory equipment adopted for the sample setup.

of the complex dielectric permittivity of both the medium surrounding the device (ε_{med}^*) and the probe material (ε_{PCB}^*). In our application, the medium is the soil/granular material (solid-air-water) and its permittivity ε_{med}^* depends only on its real permittivity (ε_{med}') and its electrical conductivity (σ_{med}) because the readout electronics operates in the range of 10 - 100 kHz [24], which is far from the frequencies at which water relaxation phenomena occur (~17 GHz).

III. Experimental Setup and Sample Preparation

In this work, we extended measurements reported in [23] by considering the impact of water electrical conductivity. Below the adopted setup and measurement system is reported, together with the procedure followed to prepare the coffee samples. The geometrical dimensions related to the experimental setup are reported in [23], such as the ones related to the mould in which the samples are prepared, the wire used to interface the sensor with the measurement instrument, and the sensor holder.

A. Experimental Setup

The hot electrode of the electrical potential source is tied to the central electrode of the PCB, capacitively coupled to the external electrode, which is connected to the ground potential. The electric field originating from the electrodes intersects the sensor materials (FR4 and Solder Mask) and the medium surrounding the sensor. The potential source is applied by using an HP4275A LCR meter (L is the electrical inductance, C is the electrical capacitance, and R is the electrical resistance). The sensor is interfaced to the LCR meter using a twisted pair wire with a total length equal to l_5, as shown in Fig. 2. The two ends on one side of the wire are soldered to the sensor pads on the top face of the sensor, one to the central electrode and the other one to one of the two pads of the external electrode. The twisted pair wire affects the measurement since it represents an additional impedance in series to the sensor. For this purpose, a calibration of the LCR-meter is performed to take into account such contribution.

The calibration is performed by using another identical couple of wires as the one soldered to the sensor: this is connected to the HP4275A and wired first as an Open Circuit and then in a Short Circuit configuration. Thus, the instrument measures the wires on each supported frequency upon these two
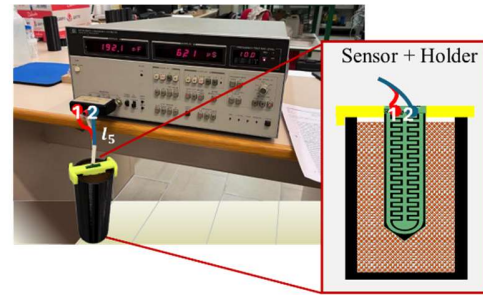
configurations and stores the data to compensate for their contribution. The signal generated by the LCR-meter to supply the sensor is a sinusoid characterized by a peak voltage level, equal to 1 V, and a frequency varying in the range of 10 kHz - 10 MHz. Four frequencies were selected, namely 10 kHz, 30 kHz, 50 kHz, and 100 kHz. The sensor is then hand-driven into the granular material which was previously compacted inside a cylindrical mould.

B. Tested Material

The tested material is an organic coffee ground characterized by an average bulk density, γ = 6.21 kN/m³, dry unit weight, γ_d, varying between 4.01 and 5.93 kN/m³ and corresponding voids ratio, e_0, in the range 1.3 – 2.4 (specific gravity, G_s = 1.365). The samples were prepared with two slightly different grain size distributions, shown in Fig. 3, namely A and B. The grain size features are also reported in Fig. 3. Type B-grain size distribution was obtained through a grinding process. For comparison, Fig. 3 also shows another set of grading curves reported in [4]. The dry unit weight is rather low (< 6 kN/m³), compared to natural soils, leading to values of initial voids ratio e_0, not lower than 1.2. Then, for each grain size distribution, the material was mixed with two different tap water, and several water content as detailed in Sect. IV. Dry samples were also tested.
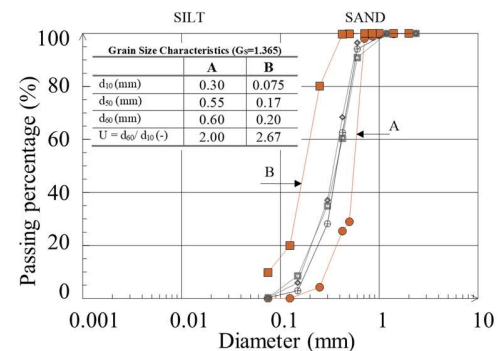
Fig. 3. Grain size distribution curves for ground coffee type A (brown with circle symbols) and ground coffee type B (brown with square symbols). The grey curves refer to data reported in [4].

C. Sample Setup and Compaction

A common procedure used to prepare wet soil samples at a certain water content involves some specific steps [1], [21]. First, a dry mass of soil is uniformly moistened by adding the required amount of water needed to reach the desired water

content. The obtained sample is then mixed and stored for a minimum of 24 hours in a controlled environment, such as a closed box or a bag, to avoid or at least reduce water evaporation. This step helps to distribute water as homogeneously as possible in the soil. Once the storage phase ends, the sample can be prepared by moist tamping method [25], to reach a specific density/voids ratio. However, for the ground coffee-material at hand, a slightly different procedure was adopted. In fact, as it is well known, the chemical behaviour of ground coffee, not already spent as in this case, is time-dependent since the dry coffee powder (see Fig. 3) reacts with water releasing caffeine as long as the powder is wet. To reduce the effects on the water dielectric constant [26] caused by the unknown molar concentration of caffeine in the sample mixture, an iterative procedure was followed to prepare the samples as quickly as possible. As a first step, the quantities of water and dry coffee powder were selected to achieve a target initial voids ratio, e_0. Two values of e_0 are considered to study the impact of density on the sensor performance. In particular, samples with coffee type A1 are prepared by considering e_0 equal to 2.00 instead of coffee type A2 and B in which the initial voids ratio was supposed equal to 1.50. In more detail, once the dry mass of coffee is determined, the weight of water equal to the first desired value of GWC percentage is added and mixed until the coffee-water mixture becomes as homogeneous as possible. Wet samples were then prepared at increasing GWCs – iteratively – by gradually adding the amount of water needed for a 5 % increase in GWC. Due to water evaporation possibly occurring during the preparation of the sample at a given GWC, particular attention is given to calculate properly the amount of coffee and water. Once a mixture is prepared, the material is then dynamically compacted inside the cylindric mould in n. 4 layers, by using a hollow cylindrical mallet of mass 853 g sliding along a vertical bar with a diameter of $\Phi = 40$ mm. For the compaction of each soil layer, the mallet is dropped between 3 and 10 consecutive times, to prepare samples at the same initial voids ratios, blowing from a height of ~17.5 cm by following a controlled and repeatable procedure. The top surface of each layer is then scarified to avoid separation between layers. The mould was crafted with a Fused Deposition Modelling (FDM) 3D printer. After sample preparation, the sensor was inserted vertically into the sample from its top surface using a PLA (*PolyLactic Acid*) handle also crafted with the 3D printer. The mould dimensions and the ones of the handle are reported in TABLE III of [23].

IV. EXPERIMENTAL RESULTS

Measurements were carried out on samples prepared by using two ground coffee materials, A and B respectively, at six increasing values of GWC. Since the electrolyte concentration affects the measurement at the frequency of interest [13], the electrical conductivity of the tap water was regularly monitored (see Section III-B). TABLE II reports the initial values of the voids ratio e_0 and porosity n_0 of two sets of A and B samples at increasing water content and highlights the electrical conductivity of the water (σ_w) used for each family of samples.

For type A, a different number of blows was used to compact the material, yielding two different target values of voids ratio (A1 and A2), and two electrical conductivities are considered (A1 and A3). Moreover, the A-type coffee is used to prepare also samples at water saturation condition, A_{Sat}, whose properties are reported in TABLE III.

TABLE II
VOIDS RATIOS AND POROSITY SAMPLE SETS

Set	A1		A2		A3		B	
σ_w (µS/cm)@20° C	578		578		130		578	
GWC (%)	e_0	n_0	e_0	n_0	e_0	n_0	e_0	n_0
0	1.98	0.66	1.58	0.61	2.00	0.67	1.31	0.57
5	2.00	0.67	1.96	0.66	2.11	0.68	1.31	0.57
10	2.19	0.69	1.49	0.59	2.13	0.68	1.39	0.58
15	2.35	0.70	1.54	0.60	2.14	0.68	1.49	0.60
20	2.31	0.70	1.54	0.60	2.13	0.68	1.62	0.62
25	2.36	0.70	1.52	0.60	2.18	0.69	1.71	0.63

TABLE III
VOIDS RATIOS AND POROSITY OF SATURATED SAMPLES A_{SAT} (σ_w=578 µS/cm)

GWC (%)	e_0	n_0	GWC (%)	e_0	n_0
0	2.00	0.67	80	2.17	0.68
10	2.10	0.68	110	2.15	0.68
20	2.07	0.67	130	2.24	0.69
50	2.20	0.69	-		

The effects of voids ratio (which is related to dry density, the larger is e_0, the lower is γ_d) and grain size distribution on impedance measurements are well analyzed in [23]. The results showed that the grain size distribution apparently exerts the higher impact. For B-type coffee samples, which are slightly finer than A-type ones, a greater material homogeneity was observed, hence minimizing the air gap which is generally formed at the soil-sensor interface [27]. Thus, the sensor features a better sensitivity when coupled to B-type samples.

Of particular importance is also the impact of electrical conductivity of the medium surrounding the sensor, which can affect both the capacitance and the conductance. For this reason, measurements were also taken in samples of A3-type (Fig. 4) approximately at the same density (porosity) of A1 type, but prepared by using a water electrical conductivity that is almost five times smaller (see TABLE II). Both capacitance and conductance measurements are affected by the electrical conductivity of the water used to moisten the ground coffee. The capacitance shows an increase in the sensitivity at all four frequencies of interest. Moreover, when the GWC increases, the conductance shows a faster attainment of the stability condition already shown in A1- type samples. The decreasing conductance behaviour for high values of GWC can be explained taking into account that the measured conductance of the planar sensor is ascribable not only to the permittivity and conductance of the external medium, but to a series admittance contribution of Solder Mask - Soil - Solder Mask. Finite Element simulations (not shown in this paper) confirm that the contributions of frequency and all physical parameters of the sensor and soil mix up yielding the displayed counterintuitive physical behaviour of the conductance, as displayed in Fig. 4.
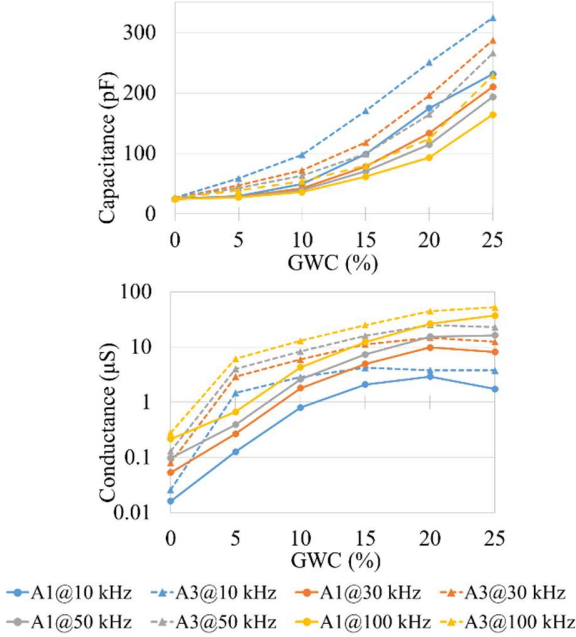
Fig. 4. Capacitance and Conductance measured by the sensor in type A1 and A3 coffee samples as a function of the GWC.

V. Measurement-based Model

Herein we present a measurement-based analytical model that expresses the capacitance and the conductance of the parallel electrical model as a function of the GWC. We present two variants of this model, the first one for unsaturated samples, and the second one for samples reaching the saturation condition. This model is then exploited to obtain an estimate of the GWC as a function of the measured values of capacitance and conductance.

A. Measurement-based Model for Unsaturated Samples

By observing the analytical shape shown by the four datasets at low levels of GWC (coffee types A1, A2, A3, and B), a function of two variables is hypothesized. The considered model for the capacitance, $C_F(\theta, \omega)$, is based on a second-order polynomial with respect to the two variables, which are the GWC, θ, and the angular frequency $\omega = 2\pi f$, where f the frequency of the signal applied to the sensor during the measurement:

$$C_F(\theta, \omega) = C_0(\omega) + a_1\theta + a_2\theta\omega + a_3\theta\omega^2 + a_4\theta^2 + a_5\theta^2\omega \quad (2)$$

$$C_0(\omega) = C_F(0, \omega) = b_1\omega^2 + b_2\omega + b_3$$

where $C_0(\omega)$ is the capacitance when the GWC is equal to 0% and the coffee ground is dry. The two parameter vectors, $a = [a_1, a_2, a_3, a_4, a_5]^T$ and $b = [b_1, b_2, b_3]^T$, are estimated using an LS approach. We assume that there is a linear dependence between the measurement vector q and the unknown parameter vector p, expressed by

$$q = Wp \quad (3)$$

where W is a matrix that expresses the linear relationship

between the parameters and the measurements. Equation (3) is combined with (2) to identify the parameter vectors a and b. By inverting (3) in the LS sense, we obtain

$$a = (W_a^T W_a)^{-1} W_a^T q_a \quad \text{and} \quad b = (W_b^T W_b)^{-1} W_b^T q_b \quad (4)$$

where $q_a = [c_{11}, \dots, c_{61}, \dots, c_{14}, \dots, c_{64}]^T$, $c_{ij} = C_M(\theta_i, \omega_j)$ is the capacitance measured at GWC θ_i (where $i = 1, \dots, 6$) and angular frequency ω_j (where $j = 1, \dots, 4$), $q_b = [c_{01}, c_{02}, c_{03}, c_{04}]^T$, $c_{0i} = C_M(0, \omega_i)$ is the measured capacitance vector in dry samples at angular frequency ω_i, and W_a and W_b are defined as

$$W_a = \begin{bmatrix} A_1 \\ A_2 \\ A_3 \\ A_4 \end{bmatrix} \qquad W_b = \begin{bmatrix} 1 & \omega_1 & \omega_1^2 \\ 1 & \omega_2 & \omega_2^2 \\ 1 & \omega_3 & \omega_3^2 \\ 1 & \omega_4 & \omega_4^2 \end{bmatrix}$$

$$A_i = \begin{bmatrix} \theta_1 & \theta_1\omega_i & \theta_1\omega_i^2 & \theta_1^2 & \theta_1^2\omega_i \\ \theta_2 & \theta_2\omega_i & \theta_2\omega_i^2 & \theta_2^2 & \theta_2^2\omega_i \\ \theta_3 & \theta_3\omega_i & \theta_3\omega_i^2 & \theta_3^2 & \theta_3^2\omega_i \\ \theta_4 & \theta_4\omega_i & \theta_4\omega_i^2 & \theta_4^2 & \theta_4^2\omega_i \\ \theta_5 & \theta_5\omega_i & \theta_5\omega_i^2 & \theta_5^2 & \theta_5^2\omega_i \\ \theta_6 & \theta_6\omega_i & \theta_6\omega_i^2 & \theta_6^2 & \theta_6^2\omega_i \end{bmatrix} \quad (5)$$

where $i = 1, \dots, 4$ is the frequency index. Note that the matrix A_i uses six values of GWC for the ith angular frequency ω_i, but the model can easily be generalized to include more values of GWC and frequencies, by increasing the dimensions of the involved matrices and vectors.

Differently from the capacitance model, the model for the conductance is hypothesized considering its normalisation to the angular frequency. Indeed, the normalised conductance, $\hat{G} = G/(\omega C_{norm})$, where $C_{norm} = 1$ F, has a weak dependency on the angular frequency. Therefore, we assume a parabolic behaviour of the normalised conductance on a log scale. The model used for the LS fitting, $\hat{G}_F(\theta)$, is reported in the equation below

$$\hat{G}_F(\theta) = 10^{d_1 + d_2\theta + d_3\theta^2} \quad (6)$$

where d_1, d_2, and d_3 are parameters to be determined. After taking the logarithm at both sides of (6), the parameter vector $d = [d_1, d_2, d_3]^T$ is estimated in the LS sense as in (2)-(4), by performing $d = (W_d^T W_d)^{-1} W_d^T q_d$, where

$$W_d = \begin{bmatrix} 1 & \theta_1 & \theta_1^2 \\ 1 & \theta_2 & \theta_2^2 \\ 1 & \theta_3 & \theta_3^2 \\ 1 & \theta_4 & \theta_4^2 \\ 1 & \theta_5 & \theta_5^2 \\ 1 & \theta_6 & \theta_6^2 \end{bmatrix} \quad (7)$$

and $q_d = [g_1, \dots, g_6]^T$, where each element g_i is obtained by averaging (over the frequency index j) the measured values of the normalised conductance $g_{ij} = \log_{10}(G_M(\theta_i, \omega_j)/(\omega_j C_{norm}))$ at GWC θ_i and angular frequency ω_j. The

parameters obtained from the model (2)-(7) on type A1, A2, A3, and B samples are reported in TABLE IV. Specifically, the table highlights that samples characterized by different working conditions are modelled with parameters that have the same order of magnitude.

TABLE IV
CAPACITANCE AND CONDUCTANCE PARAMETERS (UNSATURATED SAMPLES).

	P	A1	A2	A3	B
$C_F(\theta, \omega)$	a_1	$-2.763 \cdot 10^1$	$1.296 \cdot 10^2$	$5.419 \cdot 10^2$	$8.902 \cdot 10^2$
	a_2	$-8.486 \cdot 10^{-4}$	$-1.170 \cdot 10^{-3}$	$-2.264 \cdot 10^{-3}$	$-2.799 \cdot 10^{-3}$
	a_3	$8.863 \cdot 10^{-10}$	$8.371 \cdot 10^{-9}$	$1.641 \cdot 10^{-9}$	$1.975 \cdot 10^{-9}$
	a_4	$3.835 \cdot 10^3$	$3.732 \cdot 10^3$	$3.213 \cdot 10^3$	$4.400 \cdot 10^3$
	a_5	$-1.310 \cdot 10^{-3}$	$-1.328 \cdot 10^{-4}$	$1.355 \cdot 10^{-3}$	$1.352 \cdot 10^{-3}$
$C_0(\omega)$	b_1	$1.002 \cdot 10^{-12}$	$1.353 \cdot 10^{-12}$	$-2.515 \cdot 10^{-12}$	$1.518 \cdot 10^{-12}$
	b_2	$-1.514 \cdot 10^{-6}$	$-1.915 \cdot 10^{-6}$	$-1.175 \cdot 10^{-6}$	$-2.089 \cdot 10^{-6}$
	b_3	$2.495 \cdot 10^1$	$2.622 \cdot 10^1$	$2.739 \cdot 10^1$	$2.662 \cdot 10^1$
$\hat{G}_F(\theta)$	d_1	-6.592	-6.436	-6.180	-6.104
	d_2	$1.924 \cdot 10^2$	$2.074 \cdot 10^2$	$2.276 \cdot 10^2$	$2.327 \cdot 10^2$
	d_3	$-4.068 \cdot 10^2$	$-4.955 \cdot 10^2$	$-6.036 \cdot 10^2$	$-6.171 \cdot 10^2$

As an example, Fig. 5 shows a comparison between the experimental data in A1-type coffee samples and the modelled capacitance and conductance. Concerning the capacitance model, there is a good agreement between the measurements and the results of the proposed LS fitting. Note that the capacitance model obtained by LS fitting produces parabolas whose vertex is located in the GWC range between 0% and 10%. Therefore, if we desire to use this analytical model to estimate the GWC starting from capacitance measurements only, the estimation of GWC would be difficult in this range, because the parabolic curve has two solutions. For this reason, in Section V.C, we present a GWC estimation method that combines both the capacitance model and the normalised conductance model. For what concerns the conductance in Fig. 5, the model well describes the behaviour of the measurements, but the presence of a single curve produces a residual error that is smaller for intermediate frequencies and larger for side frequencies. This residual error is caused by the weak dependency of the normalised conductance on the angular frequency.

B. Measurement-based Model extended to include Saturation Condition

The second-order polynomial model reported in (2) could also be applied to the A_{Sat}-type samples, where experimental data have been obtained until the sample saturation condition, to properly describe the points at low GWC. However, as shown in [23], as the water content increases, the capacitance approaches a saturation condition assuming a rather constant behaviour. To well describe the capacitance measurements for high levels of water content, a double exponential model is used, and defined as follows

$$C_F(\theta, \omega) = (C_\infty(\omega) + 1) \cdot (1 - e^{\alpha\theta^\gamma + \beta\omega})$$
$$C_\infty(\omega) = k_1 \ln(\omega/\omega_{norm}) + k_2 \tag{8}$$

where α, β, γ, k_1 and k_2 are model parameters, ω_{norm}= 1 Hz and $C_\infty(\omega)$ is the capacitance corresponding to the saturation
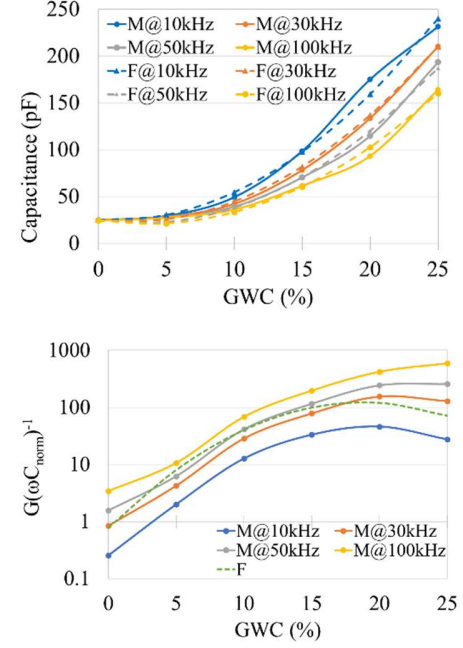

Fig. 5. Comparison between model (dashed lines) and measurements (solid lines) for capacitance and normalised conductance (type A1 coffee sample).

condition at GWC equal to 130%. The parameters k_1 and k_2 can be estimated using an LS approach. In addition, for a fixed value of γ, the parameters α and β can be estimated by using a logarithmic LS approach as done in (6). Therefore, we can repeat this procedure for different values of γ and successively select the set of parameters (α, β, γ) that minimizes the residual error. The normalised conductance model for unsaturated samples, reported in equation (6), is suitable also for the measurements done in saturated condition, provided that the GWC is between 0% and 50%. For higher values of the GWC, between 50% and 130%, the normalised conductance is modelled by the hyperbolic function

$$\hat{G}_F(\theta) = \frac{1}{h_1\theta + h_2} \tag{9}$$

where the parameters h_1 and h_2 are estimated using the LS approach of (3)-(4) applied to the set of linear relations obtained from $h_1\theta_i + h_2 = 1/\hat{G}_M(\theta_i)$, where $\hat{G}_M(\theta_i)$ is the normalised measured conductance at GWC θ_i. Note that the conductance measurement done at GWC = 50% is considered twice, in order to better match the log-parabolic model (6) at lower GWC with the hyperbolic model at higher GWC. The results of this modelling are reported in Fig. 6, while the parameters of the whole model are listed in TABLE V.

By observing Fig. 6, it is noteworthy that the model for the capacitance has a good agreement with the measurements, for all four frequencies. The second-order polynomial for low GWC finds its connection with the exponential model at a GWC close to 25%-26%. However, the continuity of the whole model is obtained only for some frequencies (30 kHz and 100 kHz): the curves for other frequencies (10 kHz and 50 kHz) show a greater discontinuity. In the case of the model at 10 kHz, the gap between the two curves occurs between 25.3% and

25.7%, corresponding to a capacitance value of 367.83 pF that
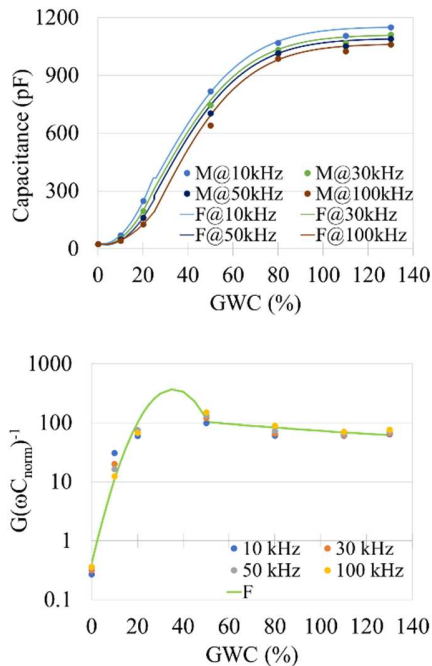
Fig. 6. Comparison between model (dashed lines) and measurements (points) for capacitance and normalised conductance (sample up to saturation condition).

TABLE V
CAPACITANCE AND CONDUCTANCE PARAMETERS (A_SAT SAMPLES). THE SUBSCRIPTS L AND H STAND FOR LOW GWC AND HIGH GWC.

	P	Value		P	Value
$C_{F,L}(\theta,\omega)$	a_1	$-1.045\cdot10^2$	$C_{F,H}(\theta,\omega)$	α	4.009
	a_2	$-1.300\cdot10^{-3}$		β	$2.946\cdot10^{-7}$
	a_3	$2.047\cdot10^{-9}$		γ	1.690
	a_4	$6.785\cdot10^3$	$\hat{G}_{F,H}(\theta)$	h_1	$8.161\cdot10^3$
	a_5	$-5.801\cdot10^{-3}$		h_2	$5.520\cdot10^3$
$C_0(\omega)$	b_1	$1.108\cdot10^{-12}$	$\hat{G}_{F,L}(\theta)$	d_1	-6.394
	b_2	$-1.614\cdot10^{-6}$		d_2	$1.666\cdot10^1$
	b_3	$2.558\cdot10^1$		d_3	$-2.342\cdot10^1$
$C_\infty(\omega)$	k_1	$-3.850\cdot10^1$	$C_\infty(\omega)$	k_2	$1.577\cdot10^{-3}$

should be considered as a threshold in the application of the models at that frequency. On the other hand, at 50 kHz the discontinuity occurs with a gap at GWC equal to 25% corresponding to a capacitance range between 257.65 pF and 276.75 pF. This gap corresponds to a small relative error (computed with respect to the mean value of the gap) equal to 3.75%. The threshold between the two models at that frequency could be found at 267.20 pF, corresponding to the mean value of the previous capacitance range. Since the whole model finds its continuity at 30 kHz and 100 kHz, the capacitance value to be considered as a threshold in these cases are 311.85 pF and 195.00 pF, respectively corresponding to a GWC of 25%. Concerning the normalised conductance, due to its non-monotonic behaviour, two intercepts are found between the models: the first one at GWC around 22%, and the second one at GWC approaching 52%. In this case, the reduced number of measurements does not allow us to choose between the two

available models in the range 20%-52%. For this reason, we chose to use the second intercept point suggesting the use of the hyperbolic model for GWC greater than 52%. In this case, the normalised conductance corresponds to 103.24 and occurs with capacitance values of 827.7 pF, 758.53 pF, 759,59 pF, and 709.70 pF at 10 kHz, 30 kHz, 50 kHz, and 100 kHz, respectively. Since the normalised conductance is non-monotonic, to discriminate between the two models, a prior check on the measured capacitance is required.

C. GWC Estimation from Experimental Data and Discussion

If we measure the capacitance only, the GWC could be easily estimated by simple inversion of the mathematical equations that express the model. However, in order to exploit at best the information embedded in capacitance and conductance measurements, we propose a GWC estimation approach based on the minimization of a cost function. The cost function is defined as follows

$$J(\theta,\omega) = (1 - w_G) \cdot |C_M(\theta,\omega) - C_F(\theta,\omega)|^2 + w_G \cdot |\hat{G}_M(\theta,\omega) - \hat{G}_F(\theta)|^2 \quad (10)$$

where w_G is a non-negative conductance weight ($0 \leq w_G \leq 1$, such that the capacitance weight results $w_C = 1 - w_G$), opportunely optimized to minimize the GWC estimation error. In (10), the values with the subscript M are obtained by measurements, whereas the values with the subscript F are obtained using the model described above. For each (w_G,ω) couple, the EGWC, $\theta_{est}(w_G,\omega)$, is given by

$$\theta_{est}(w_G,\omega) = \underset{\theta\in\Theta}{argmin}\, J(\theta,\omega) \quad (11)$$

where $\Theta = \{0.0, 0.1, 0.2, ..., \theta_{Max}\}$ % is the set of possible GWC, whereas θ_{Max} is equal to 25 % or 130 %, depending on the considered dataset. The implementation cost of the algorithm might not be negligible in terms of memory and power to carry out the processing, mainly due to the computation in (10), required for each possible value in the GWC set. However, the readout system could acquire the impedance value in-situ and then make data available in the cloud for remote elaboration, with a penalty in terms of power consumption due to the data transmission. Some considerations about power consumption have been reported in [24] for a prototype with a stand-alone readout system where power was significantly saved by exploiting the deep sleep mode functionality of the LoRa transmitting device.

Once the calibration parameters are found, the $C_F(\theta,\omega)$ and $\hat{G}_F(\theta)$ of the model can be univocally computed and stored in a look-up table. Assuming this look-up table is available, the computational cost of our algorithm can be estimated by counting the number of math operations required to compute (10). For each of the four frequencies, four products and three algebraic sums are required. Thus, the computational cost consists of $4\cdot(4+3) = 28$ math operations for each tentative value of GWC. In the value, we did not take into account the subtraction contained in the first term of the equation, e.g., $1 - w_G$. In fact, this subtraction is computed just once, at the

beginning of the algorithm, when the parameter w_G is selected. Instead of exhaustively checking all the GWC tentative values, the algorithm complexity can be reduced by using iterative minimization methods, such as steepest descent or Newton-Raphson methods. To select the final solution, eleven weights w_G are considered, with a step of 0.1. By defining the squared error as $|\theta - \theta_{est}(w_G, \omega)|^2$, the best weight w_G is selected by minimizing the Mean Squared Error (MSE), defined as the average of the squared error over all the considered GWC values and frequencies. In the case of unsaturated samples, a further average of the MSE has been performed, over all the four types of coffee specimens. In the case of unsaturated samples, the two best weights are $w_G = 0.2$ and 0.3, with an averaged MSE equal to $1.54 \cdot 10^{-4}$ and $1.63 \cdot 10^{-4}$, respectively. In contrast, in the saturated sample, the best weights are $w_G = 0.9$ and $w_G = 0.1$, with an MSE equal to $4.97 \cdot 10^{-3}$ and $5.43 \cdot 10^{-3}$, respectively.

In TABLE VI the Mean Absolute Error (MAE) on the EGWC is reported, for the saturated and unsaturated samples. We considered the MAE instead of the MSE to quickly highlight the difference between the EGWC and the reference GWC in the sample. In the table, we compare the MAE obtained for the two best couples of weights, in both saturated and unsaturated cases, with the MAE obtained when $w_G = 0.0$ or $w_G = 1.0$, corresponding to a GWC estimation made by using only the capacitance or the normalised conductance, respectively. These results show that using both capacitance and conductance measurements, in most cases, the estimation of the GWC is more accurate than using capacitance only.

TABLE VI
MAE OF THE EGWC FOR UNSATURATED AND SATURATED SAMPLES
EXPRESSED IN PERCENTAGE.

GWC (%)	w_G for Unsaturated Samples				GWC (%)	w_G for Saturated Sample			
	0.0	0.2	0.3	1.0		0.0	0.1	0.9	1.0
5	1.88	1.78	1.86	2.73	10	0.35	0.30	1.38	2.10
10	0.91	0.78	0.73	2.98	20	0.08	0.18	1.73	2.03
15	0.86	0.88	0.92	5.57	50	2.03	1.83	0.88	0.80
20	1.11	1.11	1.09	2.86	80	0.87	0.85	3.32	29.80
25	0.50	0.45	0.41	5.83	110	19.18	19.05	6.35	14.35
-	-	-	-	-	130	0.00	0.90	14.80	19.60

In our experimental results, conductance unexpectedly has a greater impact on the GWC estimate, despite the low conductivity of the water (578 μS/cm) used in the experiments. Therefore, we considered deeply the sensitive element behaviour and we found a side effect due to the vias connections. In fact, the diameter of the vias (equal to 0.5 mm) was approaching the technological limits to guarantee the full and uniform coverage of vias with the solder mask. We also verified this fact in our sensitive element by using a microscope. Then we verified the impact on the capacitance and conductance by considering different sensitive elements belonging to the same production batch. In Fig. 7 we reported the worst and best case for our batch, sensors S1 and S2 respectively. S1 features 16 out of 38 vias uncovered on each side of the sensor while S2 features all covered vias. Then we

repeated the same measurements with sensors S3 (the sensor used in all the experiments above reported in this paper and in [23] that shows only one uncovered via on the top side of the sensor) and S1 after having covered all the vias by using a protective coating (the new sensitive element is called S1-p). In the figure, we can see a big difference between the S1 and S2/S3 capacitance, whereas S2, S3, and S1-p have very similar values. The difference between the capacitance and conductance values of S2 and S3 is always lower than for S1, due to non-idealities in the production process, which can introduce variations in the case of conductance of up to 25%. We can therefore conclude that we trust the accuracy of the results obtained with sensor S3 throughout this paper.

Unfortunately, the presence of uncovered vias is completely random and their presence causes unwanted electrolytic effects when the sensor is immersed in water. Therefore, vias should be avoided in the sensitive element in contact with the medium whose humidity should be measured. The use of additional protective coating in the sensitive element layout allowed us to achieve good accuracy, with a mean error on the capacitance and the conductance values of 1.20% and 3.63%, respectively.
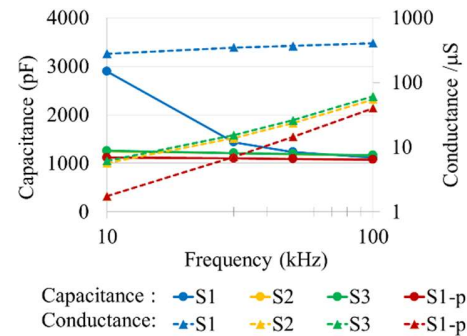

Fig. 7. Experimental results for S1, S2, S3 and S1-p sensors (S1-p indicates the recoated S1 sensor).

VI. CONCLUSION

For the particular type of granular material, i.e., ground coffee, investigated in the present paper, capacitance, and conductance measurements, even accomplished in the limited frequency range of 10 - 100 kHz, showed a rather good ability to distinguish different initial material densities (effect of voids ratio), grain size properties and water content. Different sensitivities of the sensor have also been found in different frequency ranges. We have developed a mathematical model that allows us to estimate the water content, using both capacitance and conductance, for different values of sample density. The proposed model makes it easier to estimate the water content using low-cost low-frequency IoT sensors. For future work, we foresee to use of additional measurements and artificial intelligence (AI) algorithms to further improve the accuracy of the water content estimation, e.g., by taking into account the impact of temperature and other environmental quantities. At present, we have just observed that the sensor readily reacts to any change in water content due to water evaporation from the top boundary of the material sample.

REFERENCES

[1] L. F. Ballesteros, J. A. Teixeira, and S. I. Mussatto, "Chemical, Functional, and Structural Properties of Spent Coffee Grounds and Coffee Silverskin," *Food and Bioprocess Technology*, vol. 7, no. 12, pp. 3493–3503, 2014, doi: 10.1007/s11947-014-1349-z.

[2] T. M. Mata, A. A. Martins, and N. S. Caetano, "Bio-refinery approach for spent coffee grounds valorization," *Bioresource Technology*, vol. 247, pp. 1077–1084, 2018, doi: 10.1016/j.biortech.2017.09.106.

[3] N. Zhao, Z. Liu, T. Yu, and F. Yan, "Spent coffee grounds: Present and future of environmentally friendly applications on industries-A review," *Trends in Food Science & Technology*, Vol. 143, 2024, doi: 10.1016/j.tifs.2023.104312.

[4] A. Arulrajah, F. Maghoolpilehrood, M. M. Disfani, and S. Horpibulsuk, "Spent coffee grounds as a non-structural embankment fill material: engineering and environmental considerations," *Journal of Cleaner Production*, vol. 72, pp. 181–186, 2014, doi: 10.1016/j.jclepro.2014.03.010.

[5] J.d.J. Arrieta Baldovino, R.L.dos Santos Izzo, C. Millan-Paramo "Reinforcing Spent Coffee Grounds for Geotechnical Applications", *Engineering Letters*, 30:3, EL_30_3_15, 2022, doi: 10.4322/cobramseg.2022.0016.

[6] P. A. Berbert, D.M. Queiroz, E.F. Sousa, M.B. Molina, E.C. Melo, L.R.D. Faroni, "Dielectric Properties of Parchment Coffee", Journal of *Agricultural Engineering Research*, Volume 80, Issue 1, 2001, Pages 65-80, ISSN 0021-8634, doi: 10.1006/jaer.2000.0689.

[7] N. M. Islami, Misto, Supriyadi, E. Purwandari; "Electrical properties and organoleptic test on coffee powder mixed robusta coffee and soybean.", *AIP Conf. Proc.* 20 September 2022; 2663 (1): 020003. doi: 10.1063/5.0108183.

[8] A. Tarantino, A. M. Ridley, D. G. Toll, "Field Measurement of Suction, Water Content, and Water Permeability", *Geotech Geol Eng*, Vol. 26, pp 751–782, May 2008, doi: 10.1007/s10706-008-9205-4.

[9] A. Cataldo, E. De Benedetto, G. Cannazza, E. Piuzzi and E. Pittella, "TDR-Based Measurements of Water Content in Construction Materials for In-the-Field Use and Calibration," in *IEEE Transactions on Instrumentation and Measurement*, vol. 67, no. 5, pp. 1230-1237, May 2018, doi: 10.1109/TIM.2017.2770778.

[10] E. Piuzzi *et al.*, "Measurement System for Evaluating Dielectric Permittivity of Granular Materials in the 1.7–2.6-GHz Band," in *IEEE Transactions on Instrumentation and Measurement*, vol. 65, no. 5, pp. 1051-1059, May 2016, doi: 10.1109/TIM.2015.2495720.

[11] S. Lekshmi S.U., D.N. Singh, M. S. Baghini, "A critical review of soil moisture measurement", *Measurement*, Vol. 54, pp 92–105, Apr. 2014.

[12] F. B. Poyen, S. Hazra, N. Sengupta and S. Banerjee, "Poyen's Fuzzy Logic Controlled Automatic Irrigation (FCAI): Precision Irrigation Scheduling Scheme," in *IEEE Transactions on Instrumentation and Measurement*, vol. 72, pp. 1-9, 2023, Art no. 9501109, doi: 10.1109/TIM.2022.3225909.

[13] P. Placidi, C. V. Delle Vergini, N. Papini, E. Ciancabilla, M. Cecconi and A. Scorzoni, "Soil Water Content Sensor in the IoT Precision Agriculture," *2023 IEEE SENSORS*, Vienna, Austria, 2023, pp. 1-4, doi: 10.1109/SENSORS56945.2023.10324958.

[14] Z. -y. Chang, B. P. Iliev, J. F. de Groot and G. C. M. Meijer, "Extending the Limits of a Capacitive Soil-Water-Content Measurement," in *IEEE Transactions on Instrumentation and Measurement*, vol. 56, no. 6, pp. 2240-2244, Dec. 2007, doi: 10.1109/TIM.2007.908317.

[15] M. Protim Goswami, B. Montazer and U. Sarma, "Design and Characterization of a Fringing Field Capacitive Soil Moisture Sensor," in *IEEE Transactions on Instrumentation and Measurement*, vol. 68, no. 3, pp. 913-922, March 2019, doi: 10.1109/TIM.2018.2855538.

[16] M. Chakraborty, A. Malkani and K. Biswas, "Hand-held soil moisture meter using polymer coated sensor," in *IEEE Instrumentation & Measurement Magazine*, vol. 22, no. 5, pp. 24-29, Oct. 2019, doi: 10.1109/IMM.2019.8868273

[17] P. Placidi, R. Morbidelli, D. Fortunati, N. Papini, F. Gobbi, A. Scorzoni, "Monitoring Soil and Ambient Parameters in the IoT Precision Agriculture Scenario: An Original Modeling Approach Dedicated to Low-Cost Soil Water Content Sensors," *Sensors 2021*, 21, 5110. doi: 10.3390/s21155110.

[18] P. Pal, S. Tripathi and C. Kumar, "Single Probe Imitation of Multi-Depth Capacitive Soil Moisture Sensor Using Bidirectional Recurrent Neural Network," *IEEE Transactions on Instrumentation and Measurement*, vol. 71, pp. 1-11, 2022, Art no. 9504311, doi: 10.1109/TIM.2022.3156179.

[19] M. Ni, Q. Sheng and X. Zhang, "Design and Calibration of Soil Water Content Sensor Based on Dual Frequency Excitation," in *IEEE Sensors Journal*, vol. 21, no. 24, pp. 27540-27548, 15 Dec.15, 2021, doi: 10.1109/JSEN.2021.3124785.

[20] I. Cappelli, A. Fort, M. Mugnaini, E. Panzardi, A. Pozzebon, M. Tani, "Battery-Less HF RFID Sensor Tag for Soil Moisture Measurements," in *IEEE Transactions on Instrumentation and Measurement*, vol. 70, pp. 1-13, 2021, Art no. 9504113, doi: 10.1109/TIM.2020.3036061.

[21] S. Lekshmi, D. N. Singh, A. Tarantino, M. S. Baghini, "Evaluation of the Performance of TDR and Capacitance Techniques for Soil Moisture Measurement", *Geotechnical Testing Journal*, Vol. 41, 2, Mar. 2018, doi: 10.1520/GTJ20160240.

[22] A. Cataldo et al., "Controlling the irrigation process in agriculture through elongated TDR-sensing cables," *2017 IEEE International Instrumentation and Measurement Technology Conference (I²MTC)*, Turin, Italy, 2017, pp. 1-6, doi: 10.1109/I2MTC.2017.7969761.

[23] N. Papini, M. Cecconi, P. Placidi, A. Scorzoni and A. Tarantino, "Effect of Physical Properties of Granular Sustainable-Porous Materials on Water Content Measurements by Using a Low-Cost Sensor," *2024 IEEE International Instrumentation and Measurement Technology Conference (I²MTC)*, Glasgow, United Kingdom, 2024, pp. 1-6, doi: 10.1109/I2MTC60896.2024.10561193.

[24] P. Placidi, C. V. D. Vergini, N. Papini, M. Cecconi, P. Mezzanotte and A. Scorzoni, "Low-Cost and Low-Frequency Impedance Meter for Soil Water Content Measurement in the Precision Agriculture Scenario," in *IEEE Transactions on Instrumentation and Measurement*, vol. 72, pp. 1-13, 2023, Art no. 9511613, doi: 10.1109/TIM.2023.3302898.

[25] R. S. Ladd, "Preparing Test Specimens Using Undercompaction", *Geotech. Test. J.*, 1(1): 16-23, Mar 1978, doi: 10.1520/GTJ10364J.

[26] A. R Lathi, and S. Popalghat, "Dielectric Relaxation Study of Alkaloid (Caffeine) in Aqueous Solution Using Time Domain Reflectrometry Technique", *International Journal of Science and Research (IJSR)*, Vol. 4, 5, pp. 2409-12, May 2015, doi: 10.22214/ijraset.2021.37222.

[27] T. Saito, T. Oishi, M. Inoue, S. Iida, N. Mihota, A. Yamada, K. Shimizu, S. Inumochi, and K. Inosako, "Low-Error Soil Moisture Sensor Employing Spatial Frequency Domain Transmissometry", *Sensors 2022*, 22, 8658, Aug 2022, doi: 10.3390/s22228658.